

Josephson φ_0 -junction in nanowire quantum dots

D. B. Szombati¹, S. Nadj-Perge¹, D. Car², S. R. Plissard³, E. P. A. M. Bakkers^{1,2}, L. P. Kouwenhoven¹

¹QuTech and Kavli Institute of Nanoscience, Delft University of Technology, 2600 GA Delft, The Netherlands

²Department of Applied Physics, Eindhoven University of Technology, 5600 MB Eindhoven, The Netherlands

³CNRS-Laboratoire d'Analyse et d'Architecture des Systèmes (LAAS), Université de Toulouse, 7 avenue du colonel Roche, F-31400 Toulouse, France

The Josephson effect describes supercurrent flowing through a junction connecting two superconducting leads by a thin barrier ¹. This current is driven by a superconducting phase difference φ between the leads. Due to the chiral and time reversal symmetry of the Cooper pair tunneling process ² the current is strictly zero when φ vanishes. Only if these underlying symmetries are broken the supercurrent for $\varphi = 0$ may be finite ³⁻⁵. This corresponds to a ground state of the junction being offset by a phase φ_0 . Here, for the first time, we report such φ_0 Josephson junction. Our realization is based on a nanowire quantum dot. We use a quantum interferometer device in order to investigate phase offsets and demonstrate that φ_0 can be controlled by electrostatic gating. Our results have possible far reaching implications for superconducting flux and phase defined quantum bits as well as for exploring topological superconductivity in quantum dot systems.

The process of Cooper pair tunneling through a Josephson junction (JJ) is, in general, symmetric with respect to time inversion. This has a profound consequence for the JJ current-phase relation, $I(\varphi)$. In particular it imposes the condition $I(-\varphi) = -I(\varphi)$ which in turn results in $I(\varphi = 0)$ being strictly zero. The $I(\varphi = 0) = 0$ condition is a consequence of the fact that for each process contributing to current flowing in one direction there is an opposite time reversed process, in which spin-up and spin-down electrons are reversed, that exactly cancels this current. However, time inversion is not the only symmetry which can protect the $I(\varphi = 0) = 0$ condition. For example, in JJs based on single domain ferromagnets, time inversion is broken but still the supercurrent is zero for $\varphi = 0$ due to chiral symmetry. This symmetry assures that the tunneling coefficient describing the electron tunneling forward is exactly the same as the one describing the tunneling backward. The two tunneling processes (forward and backward) cancel each other which again results in $I(\varphi = 0)$ being strictly zero. In order to create conditions for a non-zero supercurrent to flow at $\varphi = 0$, both symmetries need to be broken. Various ways were proposed theoretically to create φ_0 -junctions, including ones based on non-centrosymmetric or multilayer ferromagnets ^{3,6}, quantum point contacts ⁴, topological insulators ⁷, diffusive systems ^{8,9}, nanowires ^{10,11} and quantum dots ^{5,12,13}. In extended multi-domain ferromagnet based junctions effective built-in phase offsets were also predicted ¹⁴ and measured ¹⁵. However no experimental demonstration of φ_0 -junction was reported until now.

In quantum dots (QDs), breaking of both symmetries can possibly be achieved by the combination of an external magnetic field and spin-orbit interaction (SOI) ^{5,12,13}. Finite Zeeman splitting between spin-up and spin-down electrons breaks the time reversal symmetry. On the other hand, breaking of the chiral symmetry is more subtle. It requires interplay between the SOI and the direction of the magnetic field and it can only occur when multiple orbitals are accessible for electron transport, see Fig. 1a. When an electron goes in and out from the QD via only one orbital (Fig. 1a, upper panel) the tunneling coefficient

is exactly the same for the forward and the backward tunneling direction. As a result the chiral symmetry is preserved. If, however, the electron changes orbital within the quantum dot (Fig. 1a, lower panel), an extra phase factor is acquired in the process of orbital mixing. In this case the tunneling coefficients (matrix elements) describing forward and backward tunneling processes are necessarily complex numbers with opposite phases. Since the coefficients of the two processes are different they cannot cancel each other and the chiral symmetry is broken. Although we discussed here the case of a single electron tunneling through the QD, the same argument holds for the breaking of the chiral symmetry in the tunneling of Cooper pairs (see supplementary information and Ref 5).

The device geometry is shown in Fig. 1b and Fig. 1c. A single nanowire, made of Indium Antimonide (InSb), is contacted using Niobium Titanium Nitride (NbTiN) as a superconductor to make two JJs forming a quantum interference device (SQUID). We choose InSb nanowires due to their large spin-orbit coupling and g -factors both of which are important for breaking time inversion and chiral symmetry at relatively low magnetic fields^{16,17}. Details of the wire growth and superconducting contact deposition were reported previously¹⁸ (see also the methods section). Electrostatic gates below the wire are used to create a tunable quantum dot in the longer JJ and control the switching supercurrent of the shorter reference JJ¹⁶ (Fig. 1c). All measurements are performed at a base temperature of $T = 20$ mK in a 3-axis magnetic field where the flux through the SQUID is applied along the y direction (Fig. 1c). Standard quantum dot characterization, while the reference junction is pinched off, is used to determine the values of the charging (E_C) and orbital (E_{orb}) energies as well as g -factors. Depending on the confinement details and QD occupation number we find $E_C = 2 - 3$ meV, $E_{orb} = 0.3 - 1.5$ meV and $g = 40 - 50$ (Fig. 1d). We identify small peaks around zero bias as an onset of superconductivity and estimate the induced superconducting gap in the QD to be $\Delta^* = 20 - 50$ μ eV (see supplementary section 2).

First we measure the SQUID response in current bias for zero in-plane magnetic field (Fig. 2). Switching currents for the reference and quantum dot JJ, I_{cref} and I_{cQD} , satisfy $I_{cref} \gg I_{cQD}$, ensuring that the phase drop is mainly across the QD. The measured voltage as a function of flux and bias current I_{bias} shows oscillations with a period of $B_y = 1.2$ mT (Fig. 2a) corresponding to an effective area of $1.8 \mu\text{m}^2$, which is consistent with the SQUID geometry and the penetration depth of NbTiN ($\lambda \approx 170$ nm). Both junctions are in the phase diffusive regime such that no hysteresis is observed (Fig. 2b). This allows probing of the phase response by applying a finite $I_{bias} = 100-500$ pA close to I_{cref} and monitoring the voltage drop across the SQUID, V , as a function of gate voltage V_2 and flux Φ , see Fig. 2c and Fig. 2d as well as supplementary information section 2.

In this QD regime, the phase of the SQUID pattern depends crucially on the dot occupation number (Fig. 2b). For example, for $V_2 \approx -247$ mV, the measured voltage oscillates as a function of Φ with a particular phase (purple colored line in Fig. 2c). When V_2 is increased to around -240 mV the oscillations disappear and the overall voltage drops as the charge degeneracy point is reached. By increasing V_2 further, the oscillations recover with an extra π phase corresponding to the sign reversal of the supercurrent in a QD¹⁹ (light blue line in Fig. 2c). The change of phase by π is repeated for several consecutive charge states.

The change in phase measured for zero in-plane field occurs due to the change in the electron parity of the ground state. In a simple physical picture, for odd QD occupancy, the order of electrons forming a Cooper pair is reversed in the process of co-tunneling through a single quantum dot orbital. This results in the sign reversal of the supercurrent and the observed π shift, as previously reported in Ref.¹⁹. Note,

however, that even if the phase of the ground state is changed, $I(\varphi=0)$ remains zero which is anticipated since time reversal symmetry is preserved.

Finite magnetic fields can substantially modify this simple picture in two ways. First, the QD levels split by Zeeman energy which results in different co-tunneling rates for spin-up and spin-down electrons and therefore breaks time reversal symmetry. Second, the spin split levels belonging to different orbitals move closer in energy which enables more than one orbital to contribute to the co-tunneling process. This in turn, combined with strong SOI induced orbital mixing and asymmetry in the barriers, results in the breaking of chiral symmetry (see supplementary information 1)¹³. Under these conditions one can expect shifts in the phase by an arbitrary φ_0 .

For finite in-plane magnetic fields we find regimes in which the shifts of the SQUID pattern are different from 0 or π . Instead, the shifts take non-universal values depending on the specific QD configuration and magnetic field direction and strength (Fig. 3). Fig. 3a and Fig. 3b show an example taken close to the QD charge degeneracy point. The shift in SQUID response between the two Coulomb blockade regions is approximately 0.7π . This value is considerably different from the value π observed for the same QD regime when the in-plane field is zero (compare the data in Fig. 3a and Fig. 3b with the data in Fig. 2).

The measured gate tunable phase shift directly implies a finite φ_0 for at least one of the Coulomb blockade regions. Importantly, this shift cannot be explained by simple higher harmonic terms in the JJ current-phase relation which can occur in various semiconductor based junctions²⁰⁻²³. Even if such terms were present, as long as $I(-\varphi) = -I(\varphi)$, the SQUID response would have to be symmetric around the points corresponding to integer values of the threaded flux. Since this is clearly not the case in the data shown in Fig. 3 we conclude that the $I(-\varphi) = -I(\varphi)$ condition is violated in our QD junctions. We note that both junctions in the SQUID are nanowire based so phase shifts cannot be excluded in the reference junction as well. Hence we can only estimate relative offsets within a single junction but not the absolute value of φ_0 .

Typically, the phase of the SQUID oscillation is constant within the Coulomb blockade region and changes only at the charge degeneracy points. When the QD is strongly confined (as in Fig. 3a and Fig. 3b) the change in phase appears as a discrete jump. In this QD regime the transport at the Coulomb peak is dominated by the resonant tunneling process and therefore can be very different compared to the transport deep in the blockaded regime. For this reason we studied the QD in a more open regime as well. Interestingly, in this open QD regime we observe a continuous change in the phase of the SQUID response as we tune with the gate G_2 across the charge degeneracy point (Fig. 3c and Fig. 3d). In all regimes $B_{\text{in-plane}} \approx 50 - 150$ mT are required to observe the shift in the SQUID response (see supplementary information section 4). Note that these fields are still around two to four times smaller compared to the critical fields of $B_{\text{in-plane}} = 200-300$ mT at which the SQUID response vanishes.

Finally, we examine the magnetic anisotropy dependence of the SQUID pattern, in order to further study the microscopic origin of the φ_0 -junction. The data showing phase shifts between neighboring charge states for various in-plane magnetic field angles is presented in Fig. 4. Consistently, for many different QD regimes, we observe that the maximum shift of the SQUID pattern is most pronounced when an in-plane field is applied orthogonal to the nanowire. Previous quantum dot experiments have identified this field orientation with the preferential spin-orbit direction \mathbf{B}_{SO} for quantum dots. These measurements are consistent with SOI enabled orbital mixing which predicts maximal phase φ_0 for $\mathbf{B}_{\text{in-plane}} \parallel \mathbf{B}_{\text{SO}}$ ^{5,12,13}. We note, however, that other mechanisms, such as flux penetrating JJ area and

phase dependent tunneling, could also contribute to the additional phase shifts (see supplementary information section 3 for detailed discussion).

In summary, we demonstrated a gate tunable φ_0 -Josephson junction. Results presented here imply that the breaking of the underlying symmetries can be achieved in superconductor-quantum dot structures while maintaining coherent transport of Cooper pairs. In this context, our experiment is directly related to the efforts of studying triplet superconductivity as well as in achieving topological superconducting phase in quantum dots coupled to an s-wave superconductor^{13,24,25}. Aside from that, a gate tunable phase offset may open novel possibilities for the realization of electrically controlled flux and phase based quantum bits²⁶ as well as superconducting “phase” batteries and rectifiers^{4,27}.

Acknowledgments: We gratefully acknowledge Sergey Frolov, Dmitry Pikulin, Attila Geresdi, Kun Zuo, Vincent Mourik, Anton Akhmerov, Michael Wimmer, Y. Nazarov, and C. Beenakker for useful discussions and their help. This work has been supported by funding from the Netherlands Foundation for Fundamental Research on Matter (NWO/FOM), Microsoft Corporation Station Q and the ERC synergy grant.

Methods:

The Indium Antimonide (InSb) wires used in the experiments were grown using MOVPE process. Before superconducting contacts deposition wires were etched in Ar^+ plasma for 120 seconds to remove native surface oxides. NbTiN was sputtered in similar conditions as in Ref. 14. Finite offsets in the SQUID response corresponding to φ_0 junction were observed in three separate cooldowns of the device.

Author contributions:

D.B.S. fabricated the sample and D.B.S. and S. N-P performed the measurements. D.C., S.R.P. and E.P.A.M.B. grew the InSb nanowires. All authors discussed the data and contributed to the manuscript.

References:

1. Josephson, B. D. Possible new effects in superconductive tunnelling. *Phys. Lett.* **1**, 251–253 (1962).
2. Yip, S.-K., De Alcantara Bonfim, O. F. & Kumar, P. Supercurrent tunneling between conventional and unconventional superconductors: A Ginzburg-Landau approach. *Phys. Rev. B* **41**, 11214–11228 (1990).
3. Buzdin, A. Direct Coupling Between Magnetism and Superconducting Current in the Josephson φ_0 Junction. *Phys. Rev. Lett.* **101**, 107005 (2008).
4. Reynoso, A. A., Usaj, G., Balseiro, C. A., Feinberg, D. & Avignon, M. Anomalous Josephson Current in Junctions with Spin Polarizing Quantum Point Contacts. *Phys. Rev. Lett.* **101**, 107001 (2008).

5. Zazunov, A., Egger, R., Jonckheere, T. & Martin, T. Anomalous Josephson Current through a Spin-Orbit Coupled Quantum Dot. *Phys. Rev. Lett.* **103**, 147004 (2009).
6. Liu, J.-F. & Chan, K. S. Anomalous Josephson current through a ferromagnetic trilayer junction. *Phys. Rev. B* **82**, 184533 (2010).
7. Dolcini, F., Houzet, M. & Meyer, J. S. Topological Josephson φ_0 junctions. *Phys. Rev. B* **92**, 035428 (2015).
8. Alidoust, M. & Linder, J. φ -state and inverted Fraunhofer pattern in nonaligned Josephson junctions. *Phys. Rev. B* **87**, 060503 (2013).
9. Bergeret, F. S. & Tokatly, I. V. Theory of diffusive φ_0 Josephson junctions in the presence of spin-orbit coupling. *EPL Europhys. Lett.* **110**, 57005 (2015).
10. Yokoyama, T., Eto, M. & Nazarov, Y. V. Anomalous Josephson effect induced by spin-orbit interaction and Zeeman effect in semiconductor nanowires. *Phys. Rev. B* **89**, 195407 (2014).
11. Campagnano, G., Lucignano, P., Giuliano, D. & Tagliacozzo, A. Spin-orbit coupling and anomalous Josephson effect in nanowires. *J. Phys. Condens. Matter* **27**, 205301 (2015).
12. Dell'Anna, L., Zazunov, A., Egger, R. & Martin, T. Josephson current through a quantum dot with spin-orbit coupling. *Phys. Rev. B* **75**, 085305 (2007).
13. Brunetti, A., Zazunov, A., Kundu, A. & Egger, R. Anomalous Josephson current, incipient time-reversal symmetry breaking, and Majorana bound states in interacting multilevel dots. *Phys. Rev. B* **88**, 144515 (2013).
14. Goldobin, E., Koelle, D., Kleiner, R. & Mints, R. G. Josephson Junction with a Magnetic-Field Tunable Ground State. *Phys. Rev. Lett.* **107**, 227001 (2011).
15. Sickinger, H. *et al.* Experimental Evidence of a φ Josephson Junction. *Phys. Rev. Lett.* **109**, 107002 (2012).

16. Fasth, C., Fuhrer, A., Samuelson, L., Golovach, V. N. & Loss, D. Direct Measurement of the Spin-Orbit Interaction in a Two-Electron InAs Nanowire Quantum Dot. *Phys. Rev. Lett.* **98**, 266801 (2007).
17. Nadj-Perge, S., Frolov, S. M., Bakkers, E. P. a. M. & Kouwenhoven, L. P. Spin-orbit qubit in a semiconductor nanowire. *Nature* **468**, 1084–1087 (2010).
18. Mourik, V. *et al.* Signatures of Majorana Fermions in Hybrid Superconductor-Semiconductor Nanowire Devices. *Science* **336**, 1003–1007 (2012).
19. van Dam, J. A., Nazarov, Y. V., Bakkers, E. P. A. M., De Franceschi, S. & Kouwenhoven, L. P. Supercurrent reversal in quantum dots. *Nature* **442**, 667–670 (2006).
20. Rocca, M. L. Della *et al.* Measurement of the Current-Phase Relation of Superconducting Atomic Contacts. *Phys. Rev. Lett.* **99**, 127005 (2007).
21. Pillet, J.-D. *et al.* Andreev bound states in supercurrent-carrying carbon nanotubes revealed. *Nat. Phys.* **6**, 965–969 (2010).
22. Chang, D. E., Cirac, J. I. & Kimble, H. J. Self-Organization of Atoms along a Nanophotonic Waveguide. *Phys. Rev. Lett.* **110**, 113606 (2013).
23. Cleuziou, J.-P., Wernsdorfer, W., Bouchiat, V., Ondarçuhu, T. & Monthieux, M. Carbon nanotube superconducting quantum interference device. *Nat. Nanotechnol.* **1**, 53–59 (2006).
24. Leijnse, M. & Flensberg, K. Parity qubits and poor man’s Majorana bound states in double quantum dots. *Phys. Rev. B* **86**, 134528 (2012).
25. Fulga, I. C., Haim, A., Akhmerov, A. R. & Oreg, Y. Adaptive tuning of Majorana fermions in a quantum dot chain. *New J. Phys.* **15**, 045020 (2013).
26. Padurariu, C. & Nazarov, Y. V. Theoretical proposal for superconducting spin qubits. *Phys. Rev. B* **81**, 144519 (2010).
27. Reynoso, A. A., Usaj, G., Balseiro, C. A., Feinberg, D. & Avignon, M. Spin-orbit-induced chirality of Andreev states in Josephson junctions. *Phys. Rev. B* **86**, 214519 (2012).

Figure captions:

Figure 1. Schematics of the experiment. **a**, Schematics showing tunneling of an electron through the QD with two orbitals labelled 1 and 2 which are mixed by the SOI. The blue (red) line describes tunneling of an electron from the left (right) to the right (left) lead. When there is no change in orbital the two processes cancel each other (upper panel). In contrast when the orbital is changed during the tunneling (lower panel), due to interplay between the SOI and a magnetic field B , forward and backward tunneling processes do not cancel. In this case an extra phase χ is obtained in the process, which depends on the strength of the SOI and on $B_{\text{in-plane}}$. Note that the phase for forward and backward tunneling is different. **b**, Device schematic showing a dc-SQUID measured in a four terminal geometry. Voltages V_1 , V_2 , V_3 , and V_{ref} are applied on underlying gates to control the conductance of the JJs. **c**, Scanning electron microscopy (SEM) image of the actual device. Gates G_1 , G_2 and G_3 are used to define a quantum dot in the long JJ while G_{ref} tunes the current through the reference JJ. Orientation of the in-plane magnetic fields B_x and B_z are marked. B_y is used for tuning flux Φ through the SQUID. **d**, Current as a function of V_2 and B_x showing QD evolution of the Coulomb peak spacing in the field which gives g-factor $g_x \approx 51$. From similar data taken for B_z we obtain $g_z \approx 44$ and spin-orbit gap $\Delta_{\text{SO}} \approx 170 \mu\text{eV}$. The extracted Δ_{SO} corresponds to $l_{\text{SO}} \approx 350 \text{ nm}$ and $E_{\text{SO}} \approx 20 \mu\text{eV}$ ¹⁶. Measurements are performed in the voltage bias regime, $V_{\text{bias}} = 500 \mu\text{V}$. The dashed rectangle indicates the range of B_x for which the φ_0 -junction is observed.

Figure 2. Nanowire SQUID characterization. **a**, Voltage across the SQUID, V , as a function of bias current I_{bias} and flux Φ through the SQUID. The right panel shows V vs I_{bias} measured at $\Phi = 4 \Phi_0$ (cut along the orange dashed line). The switching current I_s separating low and high resistance regions is indicated. The lower panel shows voltage vs Φ for $I_{\text{bias}} = 450 \text{ pA}$ (cut across the green dashed line). **b**, V as a function of V_2 and Φ for $I_{\text{bias}} = 190 \text{ pA}$. The phase of the SQUID oscillations is alternating between 0 and π depending on the electron parity of the ground state of the QD. The right panel shows Coulomb peaks in the voltage bias regime. The bottom panel shows V vs. flux cuts at $I_{\text{bias}} = 195 \text{ pA}$ for $V_2 = -247 \text{ mV}$ (purple) and $V_2 = -233 \text{ mV}$ (light blue).

Fig 3. Observation of a continuous phase change in the Josephson φ_0 -junction. **a** and **c** V as a function of V_2 (V_3 in panel **c**) and Flux at fixed current bias ($I_{\text{bias}} = 470 \text{ pA}$, $B_{\text{in-plane}} = 120 \text{ mT}$ and $\theta = -135^\circ$ for panel **a**; $I_{\text{bias}} = 240 \text{ pA}$, $B_{\text{in-plane}} = 75 \text{ mT}$ and $\theta = -35^\circ$ for panel **c**). Here θ is the angle between the direction of the in-plane magnetic field and the nanowire axis. In contrast to the data taken at zero in-plane magnetic field, the phase shift of the voltage oscillations in flux is tunable with gate voltage V_2 (V_3 in panel **c**). **b** and **d**, V vs flux for values of V_2 (V_3 in panel **d**) marked by dashed lines on panels **a** and **c** showing phase shifts. In panel **b** the black curve is taken at $V_2 = -285 \text{ mV}$ and $I_{\text{bias}} = 460 \text{ pA}$ and the orange at $V_2 = -240 \text{ mV}$ and $I_{\text{bias}} = 470 \text{ pA}$. The relative offset from the two curves is $0.35 \pm 0.1 \Phi_0$. In panel **d** the curves are cuts from panel **c** taken at V_3 values of 213 mV; 218 mV; 225 mV; 229 mV. The corresponding offsets in phase compared to the top curve are $(0.1 \pm 0.05) \Phi_0$, $(0.3 \pm 0.05) \Phi_0$ and $(0.4 \pm 0.05) \Phi_0$. Note that in the QD regime shown in panel **c** and **d** we used gate G_3 for tuning.

Fig. 4 Anisotropy of the SQUID phase shift. Voltage vs. flux for different orientations of $B_{\text{in-plane}} = 120 \text{ mT}$ (**a-e**). Red and blue curves in each panel are taken at two neighboring charge occupations as in Fig 3a and the corresponding relative phase shift between is marked above each panel. The maximum shift from π was obtained when the field is perpendicular to the wire as expected from the SOI enabled

orbital mixing (see also supplementary information section 4). \mathbf{f} , phase offset as a function of angle θ between the nanowire and $B_{\text{in-plane}}$.

Figures:

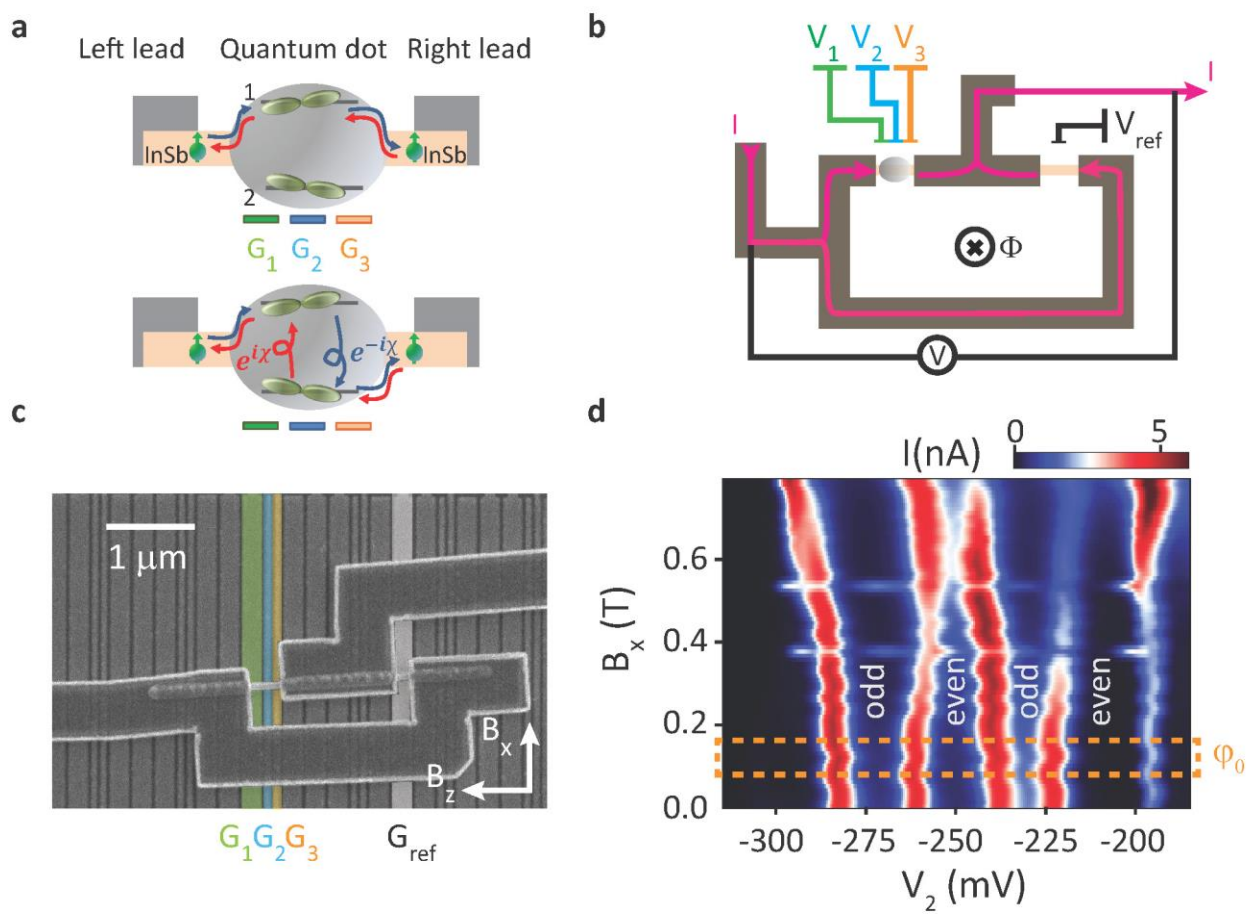


Fig. 1

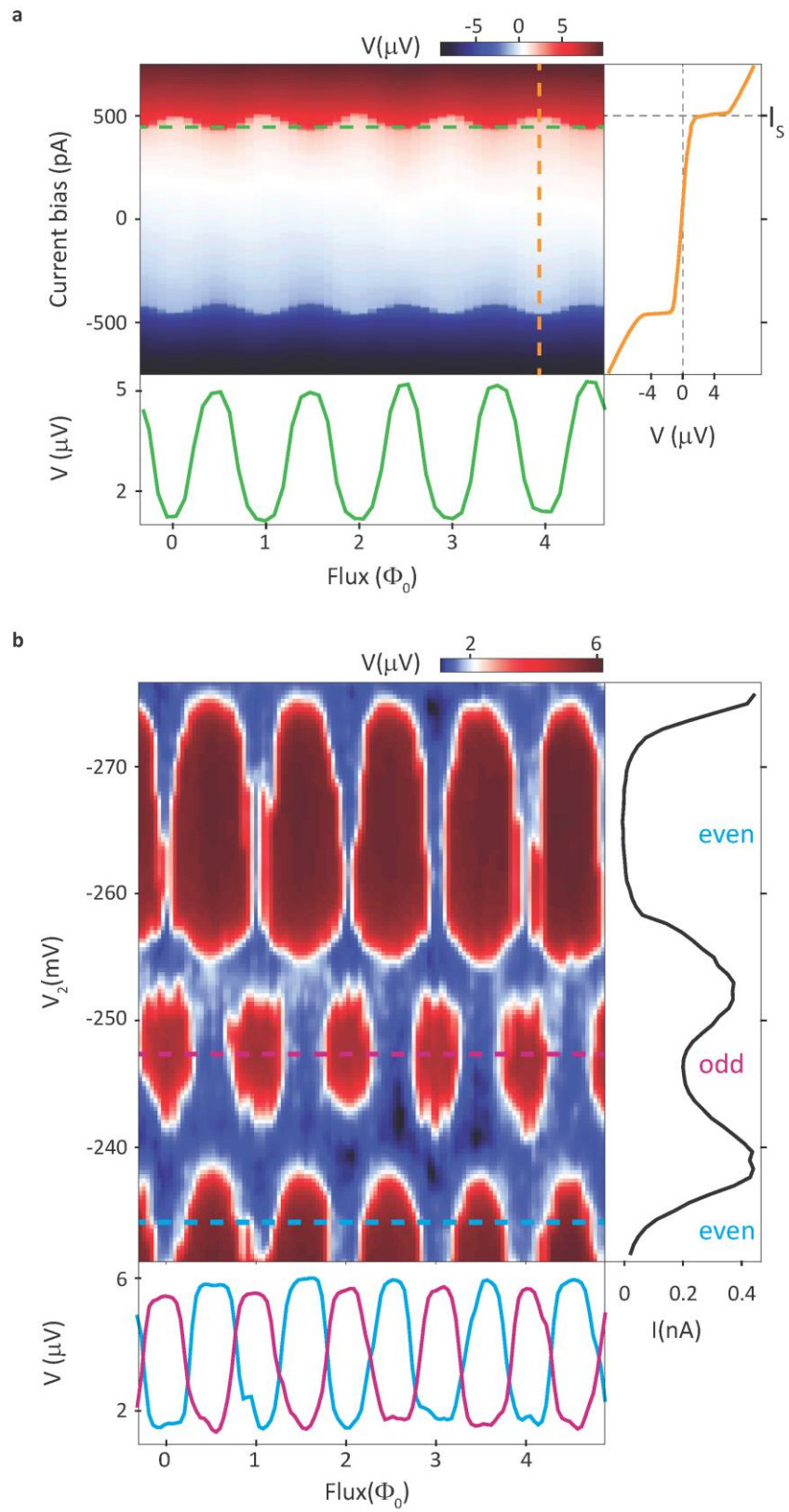


Fig. 2

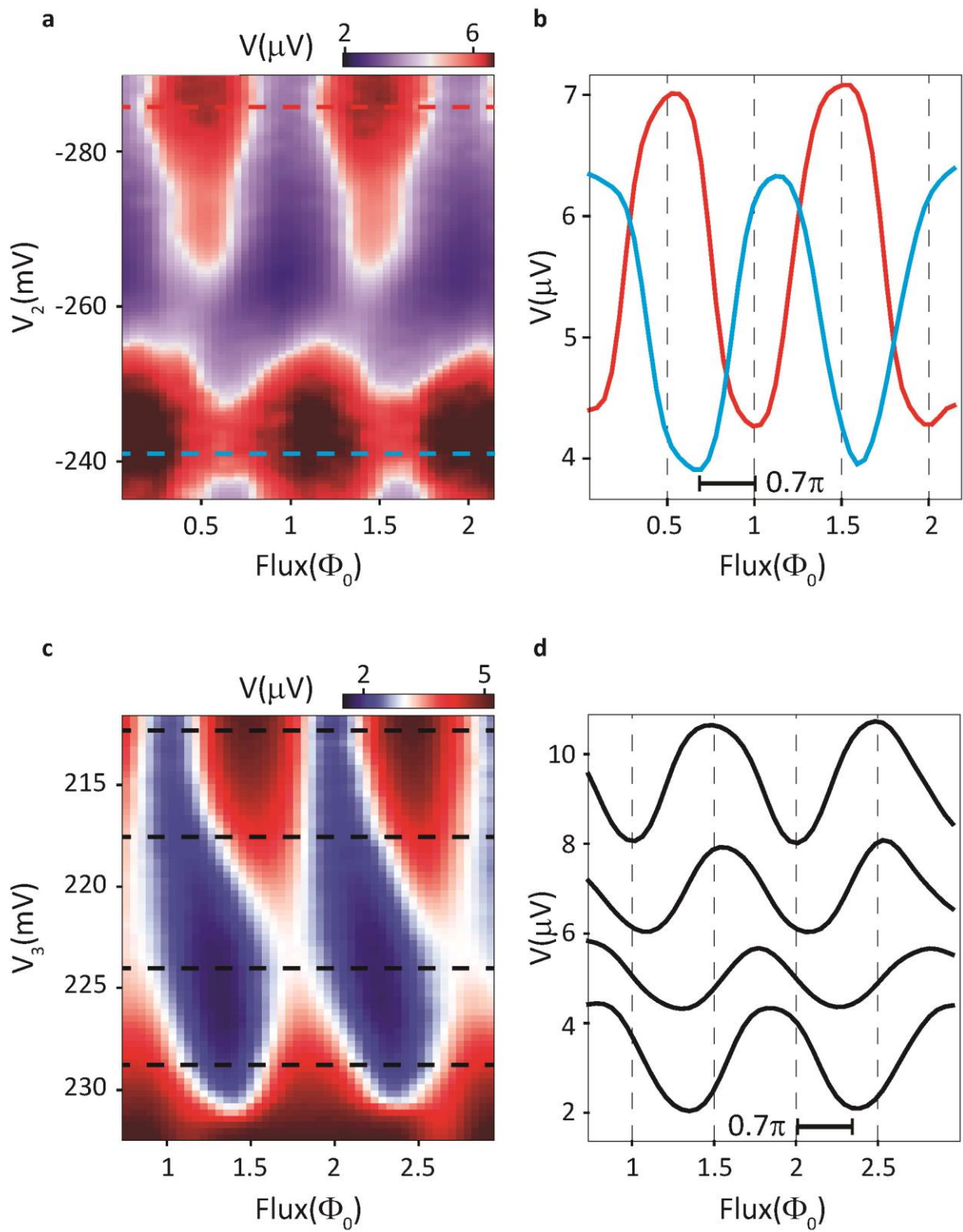


Fig. 3

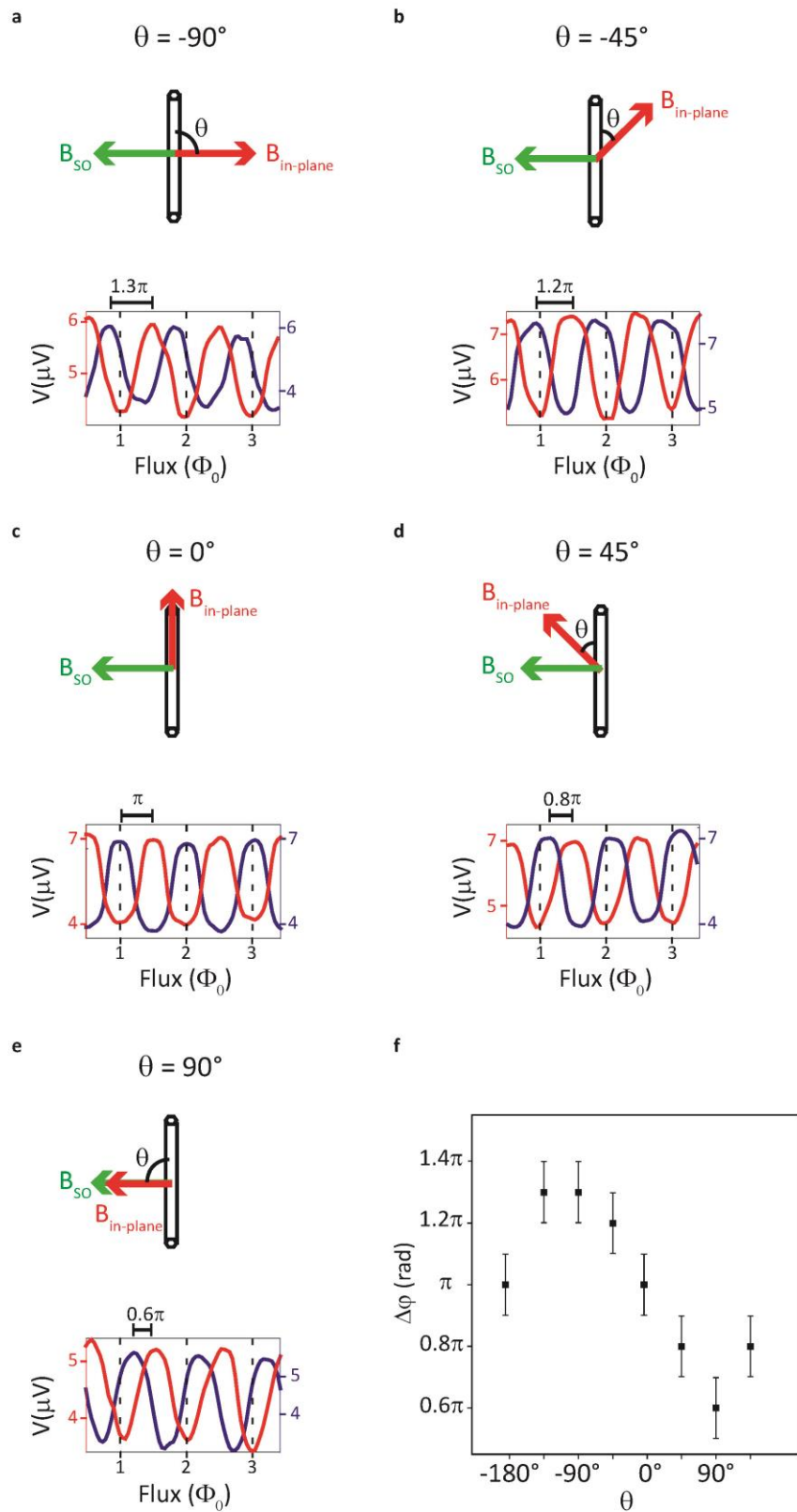


Fig. 4

Supplementary Information:

Josephson φ_0 -junction in nanowire quantum dots

D. B. Szombati, S. Nadj-Perge, D. Car, S. R. Plissard, E. P. A. M. Bakkers, L. P. Kouwenhoven

1. Breaking of the chiral symmetry in quantum dots

2. Characterization of the quantum dot junction and the nanowire based SQUID

3. Establishing the origin of the shift in the SQUID pattern

4. Additional data

1. Breaking of the chiral symmetry in quantum dots

In one-dimensional systems in which the electron momentum is well defined, the interplay between the spin-orbit interaction (SOI) and the Zeeman splitting can create a difference between the dispersion of electrons moving forward and backward. This in turn can lead to the breaking of the chiral symmetry and, in the case of superconducting transport, to Josephson φ_0 -junctions¹⁻³. In quantum dots (QDs) there is no well-defined momentum since the QD states are localized. Nevertheless, the combination of the SOI and the external magnetic field still creates similar conditions for breaking of the chiral symmetry as shown in Refs.⁴⁻⁶ and discussed below.

Let us consider a process describing a Cooper pair tunnelling from the left to the right lead (forward tunnelling) at zero phase difference. Without SOI electrons forming the Cooper pair tunnel through the QD via a single orbital level, for example the first electron tunnels via level 1 and the second via level 2. The corresponding tunnelling coefficient (matrix element) for this process is given by $(t_{L1}t_{R1})(t_{L2}t_{R2})$. Here the t_{L1} and t_{L2} (t_{R1} and t_{R2}) are the hybridization amplitudes between QD levels 1 and 2 with the left (right) lead. The terms in brackets correspond to tunnelling coefficients for individual electrons. Assuming that the hybridization amplitudes are real, the matrix element describing tunnelling from the right to the left (backward tunnelling) is exactly the same. Since the backward tunnelling contributes to the current flow in the opposite direction, the net resulting current vanishes. Therefore, the tunnelling via single orbitals can not add to $I(\varphi = 0)$. The lowest order process which contributes to $I(\varphi = 0)$ is the one in which one electron tunnels through the dot directly via a single orbital, while the other electron changes the orbital during the tunnelling process. Finite SOI enables such orbital change.

In the simplest case when two quantum dot levels contribute to Cooper pair transport and the magnetic field is orientated along the effective spin-orbit axis the Hamiltonian of the dot can be written as

$$H_{\text{QD}} = (\mu\tau_0 + E_{\text{orb}}\tau_z)\sigma_0 + B\tau_0\sigma_z + \alpha\tau_y\sigma_z \quad (1)$$

Here μ is the chemical potential, E_{orb} is the orbital energy, α parametrizes the strength of the SOI and B the Zeeman splitting, $\tau_{x,y,z}$ ($\sigma_{x,y,z}$) are Pauli matrices acting in orbital (spin) space (τ_0 (σ_0) are identity matrices). Usually the terms describing the Zeeman splitting and the SOI are smaller in comparison to the first term in the Hamiltonian. In the presence of SOI the eigenstates of the QD are mixtures of the two orbital states. The hybridization between QD eigenstates and the left (right) lead becomes $t_{L(R)1'} = t_{L(R)1} \cos \varepsilon + i \sin \varepsilon t_{L(R)2}$ and $t_{L(R)2'} = t_{L(R)2} \cos \varepsilon - i \sin \varepsilon t_{L(R)1}$ for spin-up electrons (with $\sin \varepsilon = \alpha/E_{\text{orb}}$). For the spin down electrons + and - signs should be inverted.

Importantly, due to orbital mixing, the coefficients describing tunnelling events become complex numbers implying that electrons crossing the junction gain a finite phase. This phase is opposite for the electrons tunnelling in the other direction. Therefore the forward and backward tunnelling coefficients are not exactly the same (the imaginary part is different) and the two tunnelling processes do not cancel each other. If Cooper pairs also acquire a finite phase during the tunnelling process, $I(\varphi = 0)$ becomes finite. However, if the magnetic field is zero, since spin-up and spin-down electrons obtain the opposite phases in the tunnelling process, Cooper pairs do not gain phase even when SOI is present. For finite magnetic fields the tunnelling probabilities for the tunnelling of spin-

up and spin-down electrons via different orbitals are no longer exactly the same. Only in this case can Cooper pairs obtain a finite phase.

Finally we stress that the complex tunnel coupling between superconductors always leads to finite $I(\varphi=0)$. Interestingly, this follows even from Feynman's simplified description of the Josephson effect⁷. If we assume that the wave-functions describing the two superconductors are $\psi_L = |\psi_L|e^{i\varphi_L}$ and $\psi_R = |\psi_R|e^{i\varphi_R}$, the time dependent Hamiltonian describing the superconductors on the two side of the junction can be written as

$$i\hbar \frac{\partial}{\partial t} \psi_L = \mu_L \psi_L + T \psi_R$$

$$i\hbar \frac{\partial}{\partial t} \psi_R = T^* \psi_L + \mu_R \psi_R.$$

Here μ_L and μ_R are the chemical potentials in the two superconductors and T is the tunnel coupling. Solving this set of equations for current directly gives

$$I \sim |\psi_L| |\psi_R| (\text{Re}(T) \sin(\varphi_L - \varphi_R) + \text{Im}(T) \cos(\varphi_L - \varphi_R)).$$

When T is real current is proportional to $\sin(\varphi)$, with $\varphi = \varphi_L - \varphi_R$. However if the imaginary part is non-zero, the term $\sim \cos(\varphi)$ also contributes to the current and gives rise to the finite $I(\varphi=0)$.

2. Characterization of the quantum dot junction and the nanowire based SQUID

In order to characterize the QD Josephson junction, we performed voltage and current bias measurements while the reference junction was pinched off. Depending on the exact gate configuration, the measured QD resistance varies between 40-600 k Ω and the switching currents are in the range 40-300 pA. In all measurements the sub-gap resistance is finite since the Josephson energy of the QD junction $E_J = \Phi_0 I_C / 2\pi \approx 0.5-3 \mu\text{eV}$ comparable to $k_B T \approx 5 \mu\text{eV}$. The induced gap in the QD junction is of the order of 20-50 μeV (see Fig. S2).

When the reference junction is open we observe standard SQUID oscillations. In this regime it is even easier to resolve small supercurrents of the QD junction by simply estimating the amplitude of the flux dependent voltage oscillations. Note that the data presented in the main text is taken with the SQUID tuned to the overdamped regime. However, at low magnetic fields, the SQUID is usually underdamped (Fig. S3). Due to hysteresis effects, in this case, phase offsets are difficult to track in the voltage vs flux measurements when the current bias is fixed. For this reason, before each measurement we made sure that SQUID is in the overdamped regime by tuning the switching current of the reference junction via G_{ref} .

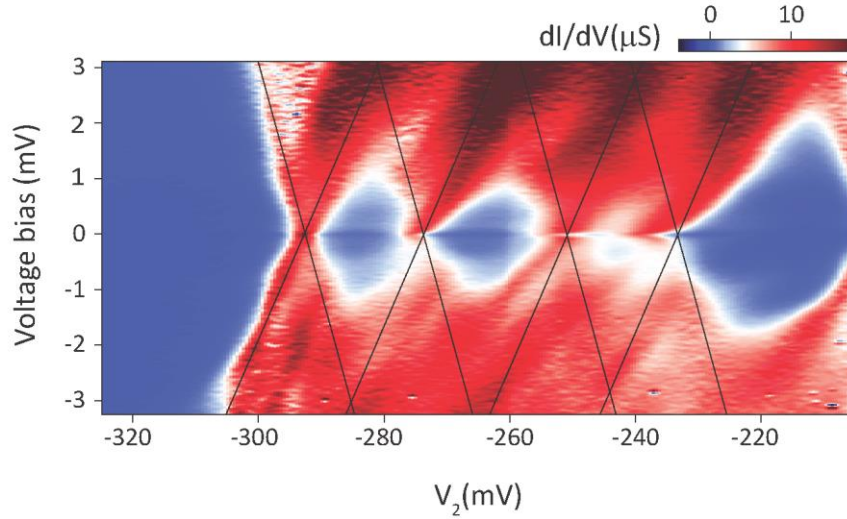


Fig. S1: Coulomb blockade diamonds for the same gate configuration as in Fig. 1 and Fig. 2 ($V_1 = 350$ mV; $V_3 = 110$ mV).

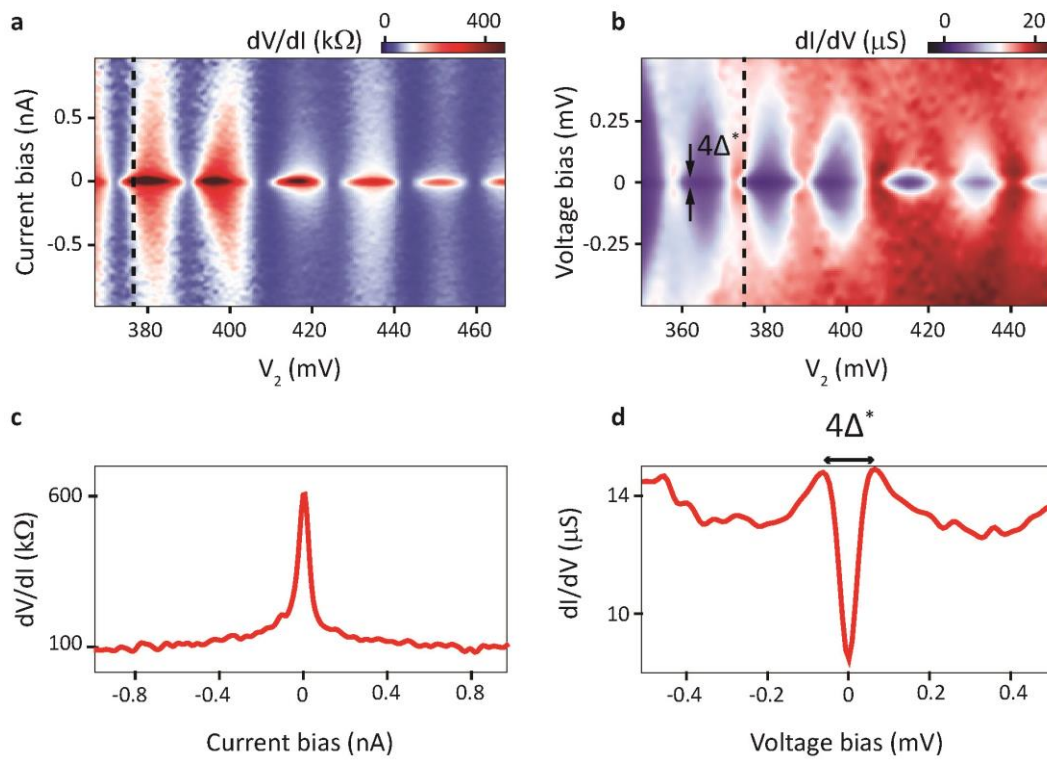


Fig. S2: Coulomb blockade in the current biased (a) and the corresponding voltage biased (b) regime ($V_1 = 350$ mV; $V_3 = 110$ mV) with V_2 being more positive. In this regime QD has ~ 30 electrons more compared to Fig. S1. c, d Linecuts for current (voltage) bias for the fixed gate voltage showing resistance (conductance) of the QD junction. The sudden increase in resistance corresponds to the suppression of the density of the states inside of the superconducting gap $\Delta^* \approx 25$ μeV in this regime. Note that the coupling between the QD and the leads is larger compared to Δ^* .

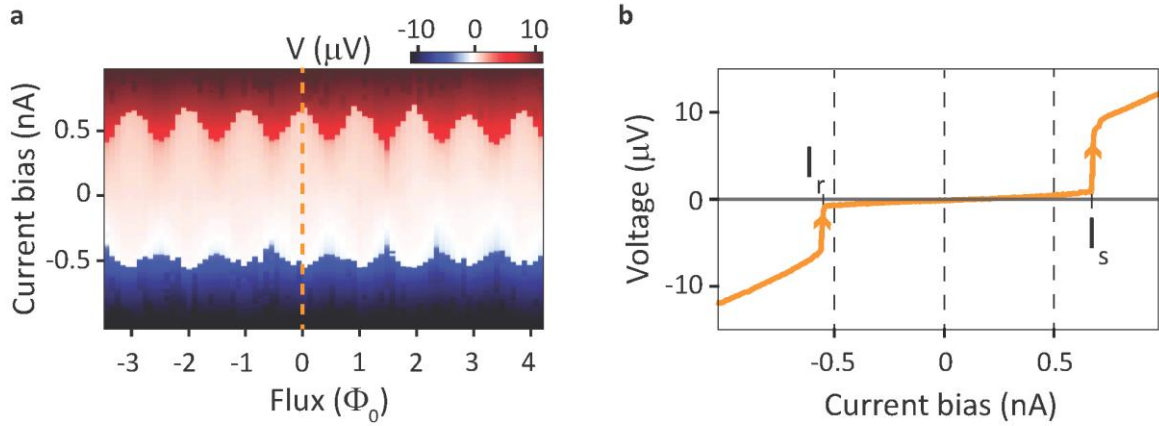


Fig. S3: SQUID in the underdamped regime at zero in-plane field ($V_1 = 100$ mV; $V_2 = 25$ mV; $V_3 = 335$ mV; $V_{\text{ref}} = 420$ mV). Left panel: Voltage as a function of flux and the current bias showing hysteresis effects in the switching and retrapping current. Right panel: line cut along the dashed line in (a) showing a difference of around 200 pA between switching and retrapping currents.

3. Establishing the origin of the shift in the SQUID pattern

Our main experimental observations can be summarized as follows: (1) The observed shift in the SQUID pattern occurs for a finite in-plane magnetic field which exact value depends on the QD configuration; (2) The shift in pattern occurs mainly for gate values at which the QD electron occupation number changes; (3) The shift is the largest when the field is orthogonal to the nanowire and almost non-existing when the field is oriented along the nanowire.

These observations are qualitatively in agreement with SOI induced orbital mixing as the origin of the φ_0 -junction. Based on (1) and (2) it is evident that QD orbital levels play a crucial role in the superconducting transport which is also in agreement with previous experiments on quantum dots⁸⁻¹⁰. Also, the observed anisotropy is consistent with reported SOI direction in QDs¹¹. In the following we discuss other effects which may also contribute to the observed shifts in the SQUID pattern.

a) Gate induced changes in the effective SQUID area. Gating off a part of the wire changes the effective SQUID area which may result in additional shifts of the interference pattern. This effect is rather small in our devices. The maximal change in the area, and therefore the phase offset, would be at most few percent estimated by comparing the gated nanowire area 100nm x 100nm with the total area of the SQUID. Even if assumed that the magnetic field is enhanced in the vicinity of the nanowire junction, due to complicated field profile caused by the nearby superconductor, the change in area has to be extremely large to account for the observed shift. Also, for substantial changes in the area, the flux periodicity of the SQUID response has to change substantially. These changes were not observed in the experiment which shows periodicity of 1.2mT being independent of the gate parameters. We also note that we didn't observe any discontinuous jumps in the interference pattern while sweeping the magnetic field which rules out phase shifts due to accidental events of flux trapping in the junction.

b) Phase offsets due to flux in the quantum dot. The observed shifts in the SQUID pattern were obtained in in-plane field values of 50-100 mT. Assuming the quantum dot area to be 60nm x 60nm (corresponding to $E_{\text{orb}} = 1.5$ meV), the total flux through the corresponding area would be of the

order of $0.1-0.2 \Phi_0$. Based on this estimate, even if the flux through the QD would fully add to the φ_0 offset, the resulting shift would be too small to explain the experimental data. Note that we verified that there is no significant modification of the field profile in the vicinity of the quantum dot by measuring values of the g -factors.

c) Additional orbital effects. Besides SOI induced orbital mixing other multi-orbital effects may contribute to the φ_0 offset. For example, the electron can acquire extra phase during the tunnelling process. In general, the matrix elements describing tunnelling in and out of different orbitals can be complex numbers corresponding to different phase factors. As shown in Ref. ^{5,6}, when the tunnelling matrices describing hybridization to the left and the right lead are complex and contribute to additional phase offsets, a finite magnetic field will result in $I(\varphi=0) \neq 0$. Also in a simple physical picture various energy differences, due to for example different g -factors in different orbitals, combined with a finite escape time from the quantum dot may result in phase factors and produce φ_0 shift. Although these effects may indeed contribute, they are to the large degree linear in magnetic field strength in contrast to the experimental data. For this reason, we can rule out these effects as the main contribution of the observed shifts.

4. Additional data

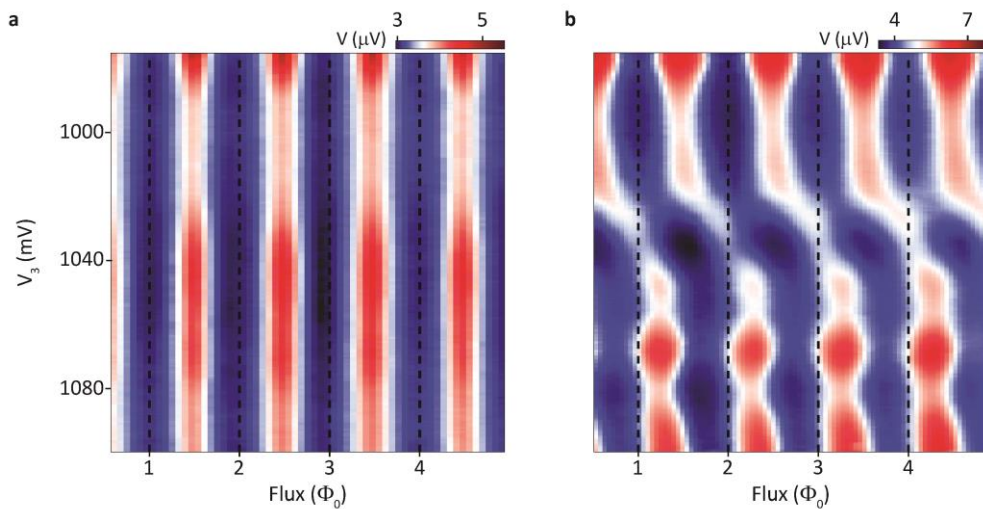


Fig. S4: Measured voltage as a function of flux and V_3 ($V_1 = 100$ mV; $V_2 = 50$ mV; $I_{\text{bias}} = 220$ pA; $V_{\text{ref}} = 450$ mV;) panel **a** at zero in-plane magnetic field and panel **b** at 150 mT, $\theta=75^\circ$. In this regime no $0-\pi$ transition is observed suggesting that multiple quantum dot orbitals contribute to the transport. The phase shifts are mainly constant inside the regions of gate space in which quantum dot occupation number is fixed.

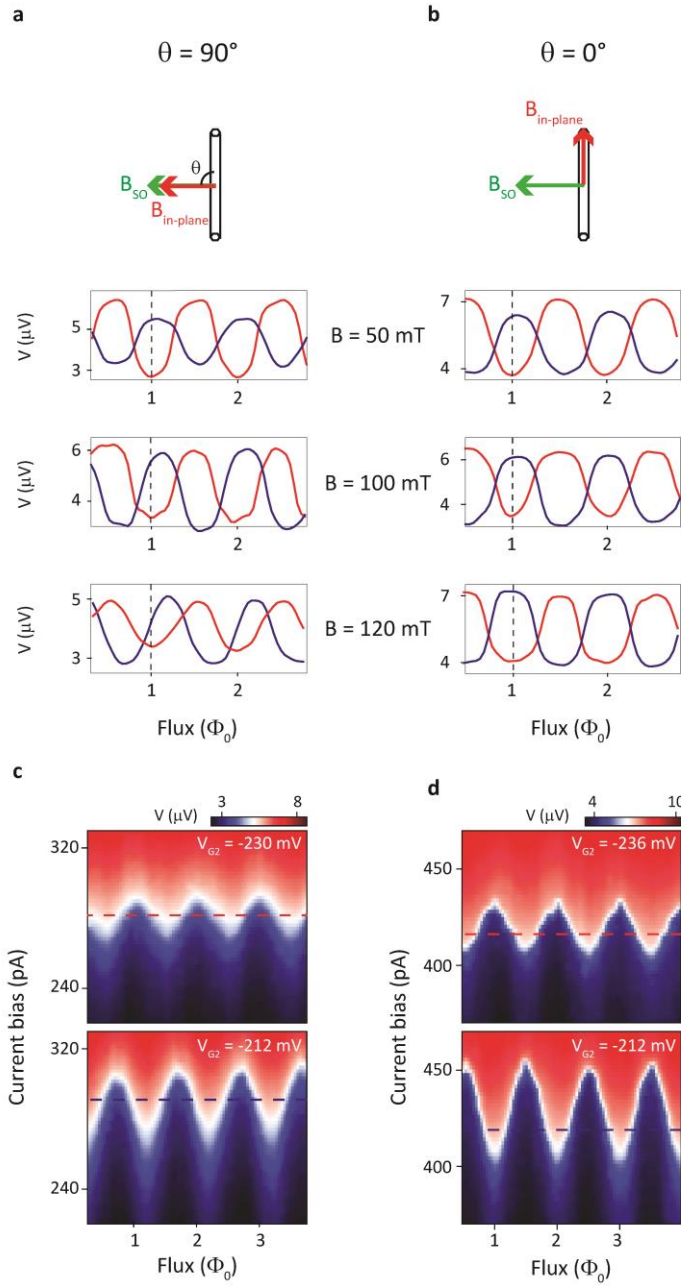


Fig. S5: Evolution of the shift in the SQUID pattern with the magnetic field for two different magnetic field orientations: **a**, orthogonal to the nanowire; **b**, along the nanowire. The blue and red trace correspond to the two consecutive quantum dot occupation states. **c**, **d** Voltage as a function of flux and current bias at $B_{\text{in-plane}} = 120$ mT for the same field orientation as in **a**, **b**. The sharp transition from the low voltage state (blue) to the high voltage state (red) indicates the value of the switching current as a function of flux. The phase offset is independent of the current bias. The red and blue lines correspond to the current bias at which the data in **a**, **b** lowest panel is taken.

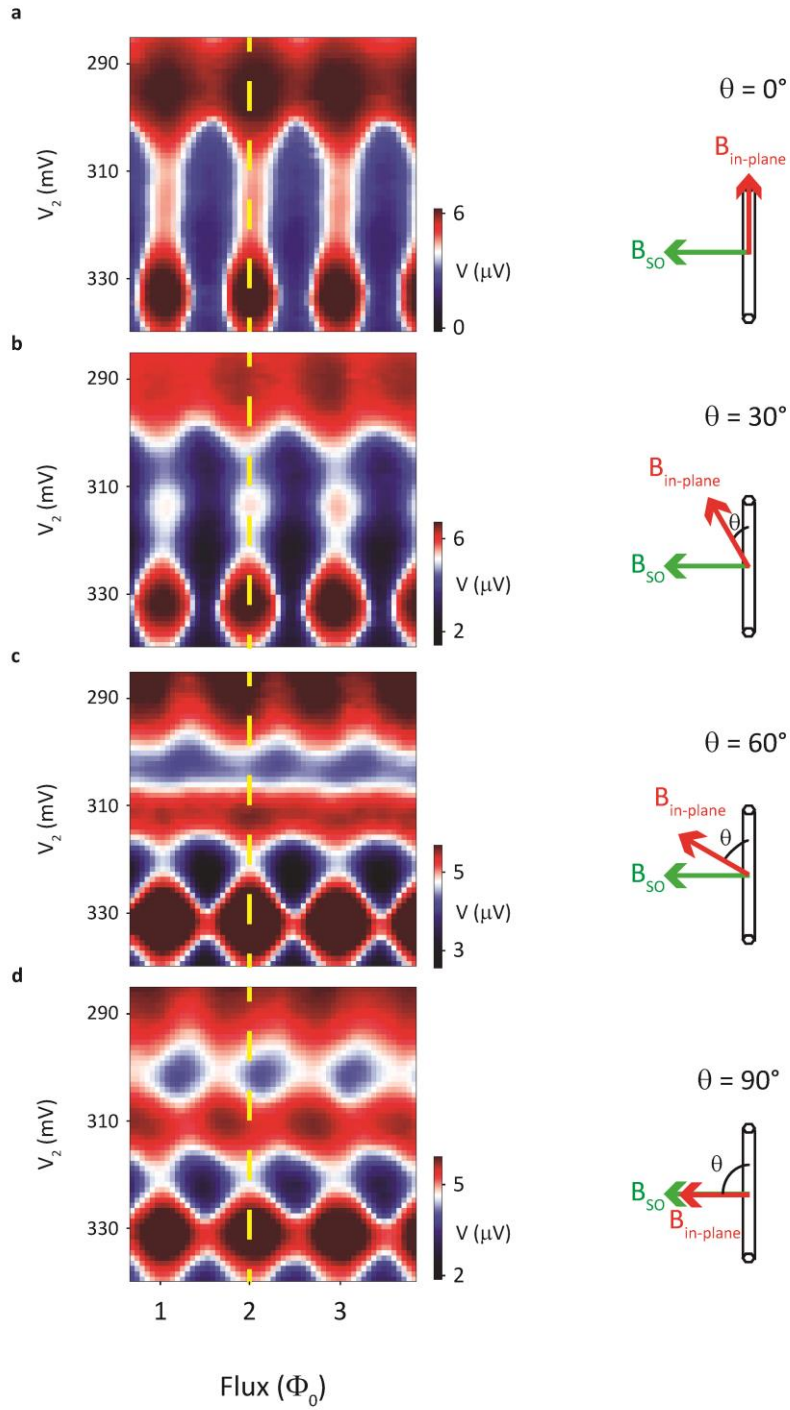


Fig. S6: Anisotropy of the SQUID phase shift in the open QD regime. Voltage as a function of V_2 and flux for different orientations of an in-plane magnetic field (**a-d**) and **30-50** more electrons compared to the regime in Fig. 4. Here the $0-\pi$ transition was not observed strongly suggesting that multiple orbitals are contributing to the transport. In this very different regime compared to the data discussed in the main text the φ_0 shifts are still the largest when the external in-plane field ($B_{\text{in-plane}}=100\text{mT}$) is oriented orthogonal to the nanowire.

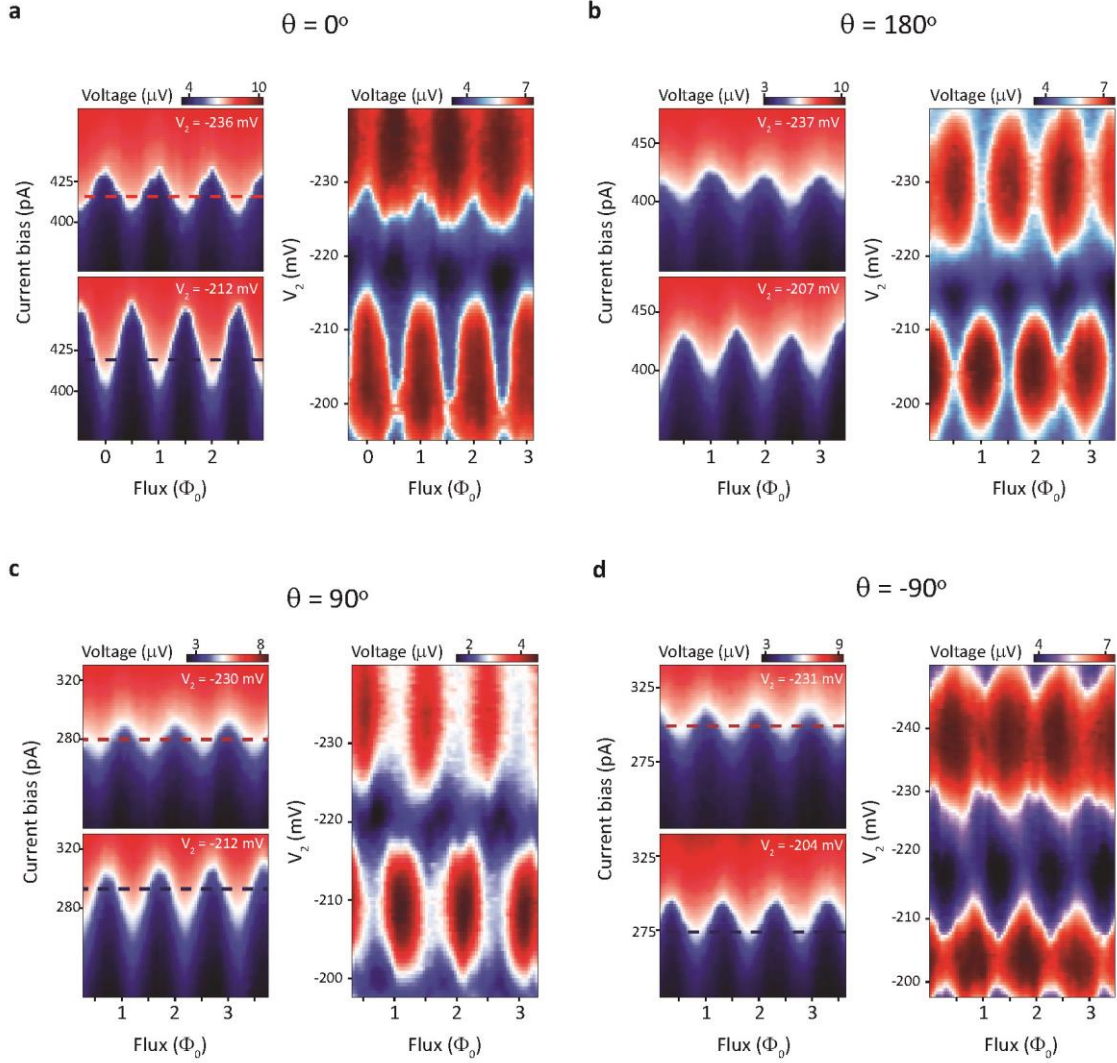


Fig. S7: Additional anisotropy data for $B_{\text{in-plane}} = 120$ mT. The left panel in **a-d** shows voltage vs current bias and flux for the gate settings corresponding to two consecutive Coulomb blockade regions. The right panel shows voltage vs V_2 and flux. Angle θ between the nanowire and the $\mathbf{B}_{\text{in-plane}}$ is indicated. Blue and red dashed lines indicate cuts shown in Fig. 4. The corresponding values of the I_{bias} are: **(a)** top panel $I_{\text{bias}} = 415$ pA , bottom panel $I_{\text{bias}} = 420$ pA; **(c)** $I_{\text{bias}} = 280$ pA, $I_{\text{bias}} = 290$ pA; **(d)** $I_{\text{bias}} = 295$ pA, $I_{\text{bias}} = 275$ pA.

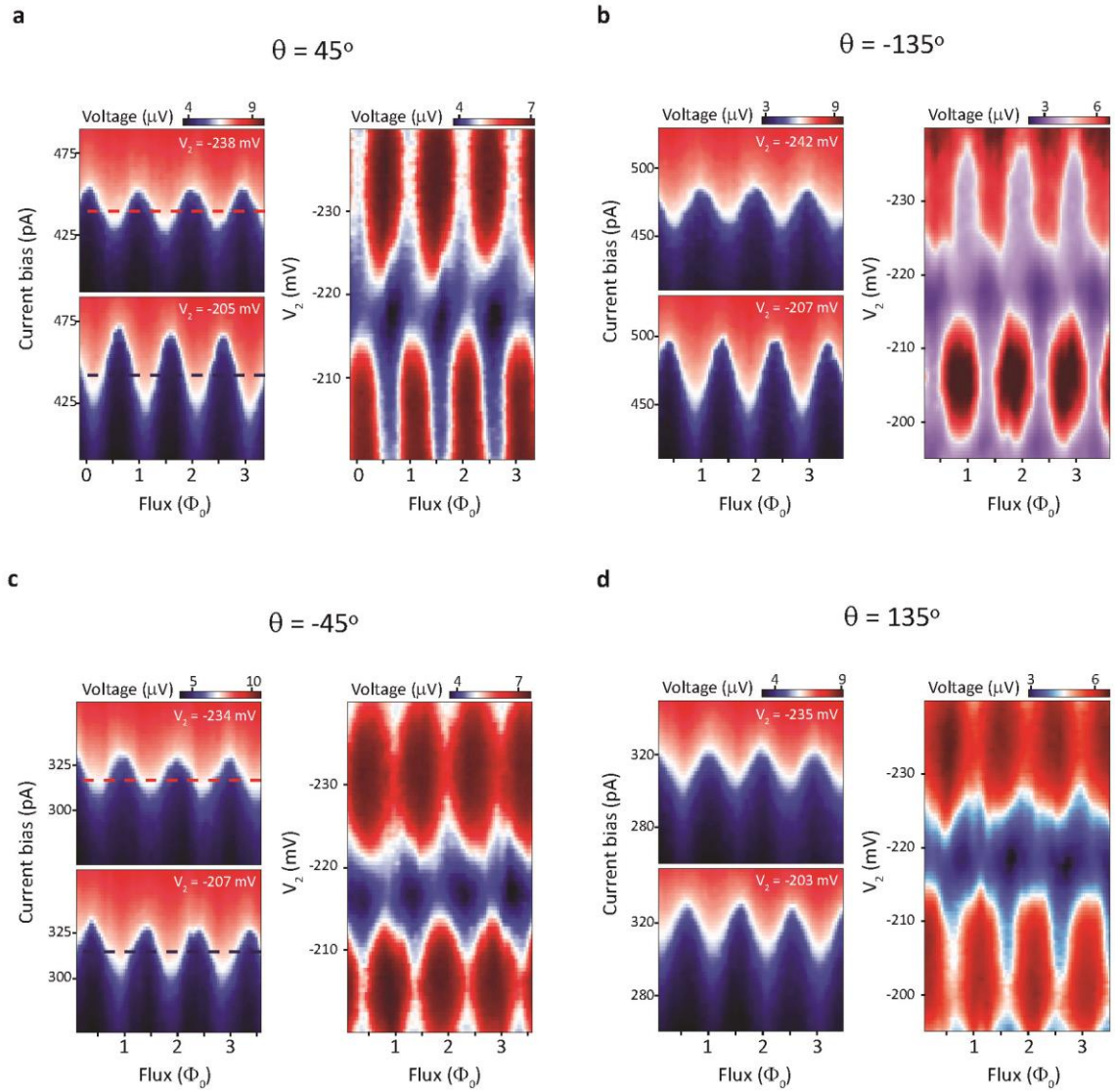


Fig. S8: Additional anisotropy data for $B_{\text{in-plane}} = 120$ mT. The Left panel in **a-d** shows voltage vs current bias and flux for the gate settings corresponding to two consecutive Coulomb blockade regions. The right panel shows voltage vs V_2 and flux. Angle θ between the nanowire and the $B_{\text{in-plane}}$ is indicated. Blue and red dashed lines indicate cuts shown in Fig. 4. The corresponding values of the I_{bias} are: **(a)** top panel $I_{\text{bias}} = 440$ pA , bottom panel $I_{\text{bias}} = 440$ pA; **(c)** $I_{\text{bias}} = 320$ pA, $I_{\text{bias}} = 315$ pA.

References:

1. Reynoso, A. A., Usaj, G., Balseiro, C. A., Feinberg, D. & Avignon, M. Anomalous Josephson Current in Junctions with Spin Polarizing Quantum Point Contacts. *Phys. Rev. Lett.* **101**, 107001 (2008).
2. Yokoyama, T., Eto, M. & Nazarov, Y. V. Anomalous Josephson effect induced by spin-orbit interaction and Zeeman effect in semiconductor nanowires. *Phys. Rev. B* **89**, 195407 (2014).
3. Dolcini, F., Houzet, M. & Meyer, J. S. Topological Josephson φ_0 junctions. *Phys. Rev. B* **92**, 035428 (2015).
4. Dell'Anna, L., Zazunov, A., Egger, R. & Martin, T. Josephson current through a quantum dot with spin-orbit coupling. *Phys. Rev. B* **75**, 085305 (2007).
5. Zazunov, A., Egger, R., Jonckheere, T. & Martin, T. Anomalous Josephson Current through a Spin-Orbit Coupled Quantum Dot. *Phys. Rev. Lett.* **103**, 147004 (2009).
6. Brunetti, A., Zazunov, A., Kundu, A. & Egger, R. Anomalous Josephson current, incipient time-reversal symmetry breaking, and Majorana bound states in interacting multilevel dots. *Phys. Rev. B* **88**, 144515 (2013).
7. Feynman, R. P., Leighton, R. B. & Sands, M. *THE FEYNMAN LECTURES ON PHYSICS, Vol III, Quantum Mechanics*. (Addison-Wesley Publishing Company, Inc., 1965).
8. van Dam, J. A., Nazarov, Y. V., Bakkers, E. P. A. M., De Franceschi, S. & Kouwenhoven, L. P. Supercurrent reversal in quantum dots. *Nature* **442**, 667–670 (2006).
9. Jarillo-Herrero, P., van Dam, J. A. & Kouwenhoven, L. P. Quantum supercurrent transistors in carbon nanotubes. *Nature* **439**, 953–956 (2006).
10. De Franceschi, S., Kouwenhoven, L., Schönenberger, C. & Wernsdorfer, W. Hybrid superconductor-quantum dot devices. *Nat. Nanotechnol.* **5**, 703–711 (2010).

11. Nadj-Perge, S. *et al.* Spectroscopy of Spin-Orbit Quantum Bits in Indium Antimonide Nanowires. *Phys. Rev. Lett.* **108**, 166801 (2012).